Stabilization of isolated attosecond pulse by controlling the emission time of high-order harmonics

Journal of Physics Communications

PAPER

Stabilization of isolated attosecond pulse by controlling the emission time of high-order harmonics

M Qin[1,2,3] and D E Kim[1,2]

[1] Department of Physics, Center for Attosecond Science and Technology, Pohang University of Science and Technology, Pohang, 37673, Republic of Korea
[2] Max Planck Center for Attosecond Science, MPK, POSTECH, Pohang, 37673, Republic of Korea
[3] Laboratory for Optical Information Technology, Wuhan Institute of Technology, Wuhan 430205, People's Republic of China

E-mail: kimd@postech.ac.kr

Keywords: high-order harmonic generation, isolated attosecond pulse, high-order harmonic emission time, three-color multi-cycle field

OPEN ACCESS

RECEIVED
1 December 2017

REVISED
6 February 2018

ACCEPTED FOR PUBLICATION
19 February 2018

PUBLISHED
1 March 2018

Abstract

Features of an isolated attosecond pulse generated by three-color fields are investigated as a function of the time delays between different-frequency components. It is found that there is a window for the time delays in which the characteristics of an isolated attosecond pulse are relatively stable. By analyzing the variation of the driving field and the harmonic emission time with the time delays, the stability of the isolated attosecond pulse is well explained. This analysis shows that by confining the harmonic emission time in a half-cycle, the sensitivity of an isolated attosecond pulse to the shift of time delays can decrease, which is important to the ultrafast measurement with an isolated attosecond pulse.

1. Introduction

Since the demonstration of an isolated attosecond pulse by high-order harmonic generation (HHG) in 2001 [1], the time-resolved spectroscopy has been extended to the attosecond domain, helping us better understand the ultrafast electron dynamics in gaseous atoms [2–6], molecules [7–10], and condensed-matter systems [11–14]. As a pump or probe tool of the spectroscopy, any change of an isolated attosecond pulse, including its pulse duration, pulse intensity and averaged photon energy, may lead to different observation results and finally to a different conclusion. Hence the stability of an isolated attosecond pulse is vital for measuring, revealing and controlling the ultrafast dynamics.

To produce a stable isolated attosecond pulse by HHG, it is necessary that the electric field waveform of the driving laser is stable from pulse to pulse. This requirement can be achieved by an extremely short laser pulse with a stabilized carrier-envelop phase (CEP) [15, 16]. However, a disadvantage of this one-color scheme is that the harmonic efficiency is severely limited [17]. Moreover, a few-cycle laser system in general is difficult to operate and maintain [18]. To improve the scheme for isolated attosecond pulse generation, researchers proposed polarization gating method [19–23] and two-color polarization gating method [24]. With the two-color polarization gating method, the harmonic efficiency was improved [24]. Whereas, the conversion efficiency remains to be further improved. It has been shown that the harmonic conversion efficiency can increase significantly if the laser's waveform is optimized by synthesizing two- or three-color fields [9, 25, 26]. In addition, many works have also been done to optimize the shape of the three-color field for harmonic extension and ultrashort attosecond pulse generation [27–30]. As for these multi-color scheme, the stability of an isolated attosecond pulse generated by the synthesized fields have not been discussed seriously.

In this paper, we investigate the features of an isolated attosecond pulse by a three-color multi-cycle long pulses and examine the stability of its characteristics respect to the time delays between different colors. The characteristics of an isolated attosecond pulse include its pulse duration, pulse intensity, and averaged photon energy. Two cases without and with phase compensation are considered here. It is found that there is a window for time delay in which an isolated attosecond pulse is relatively stable. By analyzing the variation of the electric

field and the harmonic emission time with the time delay, the stability of the isolated attosecond pulse is well explained. Our analysis shows that by confining the harmonic emission time in a half-cycle, the sensitivity of an isolated attosecond pulse to the shift of time delays can decrease.

2. Theoretical model

The high-order harmonic generation is simulated by using the strong field approximation (SFA) model [31]. This widely used SFA model can provide analytical and fully quantum-mechanical formulations for simulating the process of high-order harmonic generation. Although it does not contain the influence of the Coulomb potential of the parent ion, it has made a big success in describing and predicting the properties of the high-order harmonics. Within this model and the single active electron (SAE) approximation, the time-dependent dipole velocity is given by

$$\mathbf{v}_{dip}(t) = i\int_{-\infty}^{t} dt'\left[\frac{\pi}{\zeta + i(t-t')/2}\right]^{\frac{3}{2}} \exp[-iS_{st}(t',\, t)] \times \mathbf{E}(t') \cdot \mathbf{d}_{ion}[\mathbf{p}_{st}(t',\, t) + \mathbf{A}(t')] \times \mathbf{v}^{*}_{rec}[\mathbf{p}_{st}(t',\, t) + \mathbf{A}(t)] + c.c. \tag{1}$$

In this equation, ζ is a positive constant. t' and t correspond to the ionization and recombination time of the electron, respectively. $\mathbf{E}(t)$ refers to the electric field of the driving laser, and $\mathbf{A}(t)$ is its associated vector potential. $\mathbf{d}_{ion}[\mathbf{v}]$ and $\mathbf{v}_{rec}[\mathbf{v}]$ are the ionization dipole moment and the recombination dipole velocity, respectively. $\mathbf{p}_{st}$ and S_{st} are the stationary momentum and the quasi-classical action, which are given by

$$\mathbf{p}_{st}(t',\, t) = -\frac{1}{t-t'}\int_{t'}^{t} \mathbf{A}(t'')dt'' \tag{2}$$

and

$$S_{st}(t',\, t) = \int_{t'}^{t}\left(\frac{[\mathbf{p}_{st} + \mathbf{A}(t'')]^2}{2} + I_p\right)dt'' \tag{3}$$

with I_p being the ionization energy of the state from which the electron is ionized. Then the complex amplitude of the high-order harmonics with a frequency ω_n is obtained by

$$\tilde{\mathbf{S}}(\omega_n) = \int e^{i\omega_n t}\frac{d}{dt}\mathbf{v}_{dip}(t)\,dt. \tag{4}$$

The intensity and phase of the harmonics are calculated by using $P(\omega_n) = |\tilde{\mathbf{S}}(\omega_n)|^2$ and $\phi(\omega_n) = arg(\tilde{\mathbf{S}}(\omega_n))$, respectively. In the case without phase compensation, the attosecond pulse produced by filtering the harmonics from ω_n to ω_m is given by

$$I(t) = \left|\int_{\omega_n}^{\omega_m} \tilde{\mathbf{S}}(\omega)e^{-i\omega t}d\omega\right|^2. \tag{5}$$

For the case with phase compensation, the attosecond pulse is given by

$$I(t) = \left|\int_{\omega_n}^{\omega_m} |\tilde{\mathbf{S}}(\omega)|e^{-i\omega t}d\omega\right|^2. \tag{6}$$

The averaged photon energy of the attosecond pulse is calculated by

$$Ep = \int_{\omega_n}^{\omega_m} \hbar\omega|\tilde{\mathbf{S}}(\omega)|^2 d\omega \Big/ \int_{\omega_n}^{\omega_m} |\tilde{\mathbf{S}}(\omega)|^2 d\omega. \tag{7}$$

3. Results and discussions

We consider a three-color laser field synthesized by three linearly polarized near-infrared fields. The corresponding electric field is expressed as

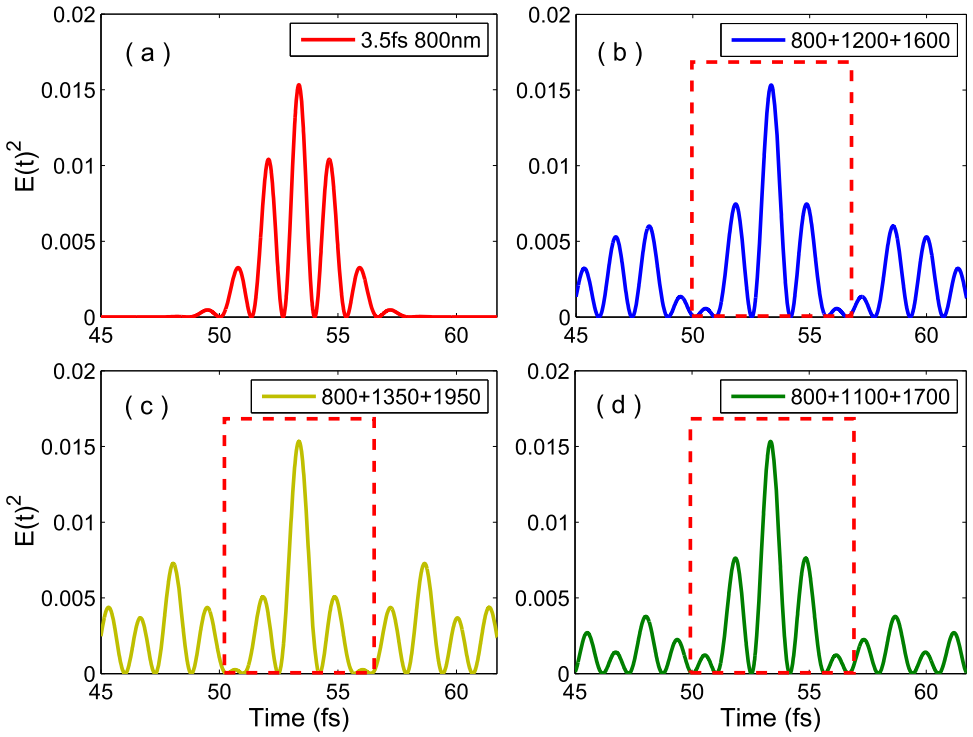

Figure 1. (a) A few-cycle laser field at wavelength of 800 nm. The pulse duration is 3.5 fs defined by the full width at half maximum. (b–c) Few-cycle-like laser fields synthesized by three color fields with a pulse duration of 28 fs. The component wavelengths are 800 nm + 1200 nm + 1600 nm for panel b, 800 nm + 1350 nm + 1950 nm for panel c, and 800 nm + 1100 nm + 1700 nm for panel d, respectively. For all these synthesized fields, the intensities of the three components are 1.5×10^{14} W cm^{-2}, 0.3×10^{14} W cm^{-2}, and 0.3×10^{14} W cm^{-2}, respectively. The time delays between different components are zero.

$$\begin{aligned} \mathbf{E}^{3c}(t) = {} & E_0 \exp\left(-2ln2\frac{t^2}{\tau_0^2}\right)\cos(\omega_0 t + \varphi_0) \\ & + E_1 \exp\left(-2ln2\frac{(t-\text{delay}_1)^2}{\tau_1^2}\right)\cos(\omega_1(t-\text{delay}_1) + \varphi_1) \\ & + E_2 \exp\left(-2ln2\frac{(t-\text{delay}_2)^2}{\tau_2^2}\right)\cos(\omega_2(t-\text{delay}_2) + \varphi_2) \end{aligned} \quad (8)$$

Where, E_i, τ_i, ω_i, and $\varphi_i (i = 0, 1, 2)$ are the electric field amplitude, pulse duration, angular frequency, and carrier-envelop phase of each component of the synthesized field. The wavelength of the fundamental field ω_0 is fixed at 800 nm. The wavelengths of the two control fields are longer than that of the fundamental field and are tuned in the near-infrared regime, which can be achieved by optical parametric amplification (OPA) or optical parametric chirped pulse amplification (OPCPA) technology [32, 33].

In figures 1(b)–(d), three different cases of the synthesized field are presented. The wavelengths of all the components are indicated in each figure. For these three cases, the intensities of the three components ω_0, ω_1, and ω_2 are 1.5×10^{14}, 0.3×10^{14}, and 0.3×10^{14} W cm^{-2}, respectively. The pulse durations of the three components are $\tau_0 = \tau_1 = \tau_2 = 28$ fs, which is defined by the full width at half maximum (FWHM). The carrier-envelop phases are $\varphi_0 = \varphi_1 = \varphi_2 = 0$. The time delay between different components are $\text{delay}_1 = \text{delay}_2 = 0$. The difference among the three cases is the different wavelength of the second and third components ω_1 and ω_2. For comparison, we also present a few-cycle laser pulse with a wavelength of 800 nm in figure 1(a). The pulse duration (FWHM) is 3.5 fs. The electric field is given by

$$\mathbf{E}^{1c}(t) = (E_0 + E_1 + E_2)\exp\left(-2ln2\frac{t^2}{\tau_0^2}\right)\cos(\omega_0 t + \varphi_0) \quad (9)$$

This equation ensures that the peak intensities of the one-color and three-color fields are the same.

Interestingly, the central parts of the synthesized electric fields, denoted by the red-dashed rectangles in figures 1(b)–(d), present a few-cycle-like structure, as in figure 1(a) for the one-color 3.5 fs field. Moreover, for all the three cases shown in figures 1(b)–(d), the peaks nearby the highest peak of the squared amplitude of the synthesized fields are suppressed significantly, due to the modulation by the second and third control fields. This property will lead to a very broad quasi-continuum spectrum, as will be discussed in the following. By scanning

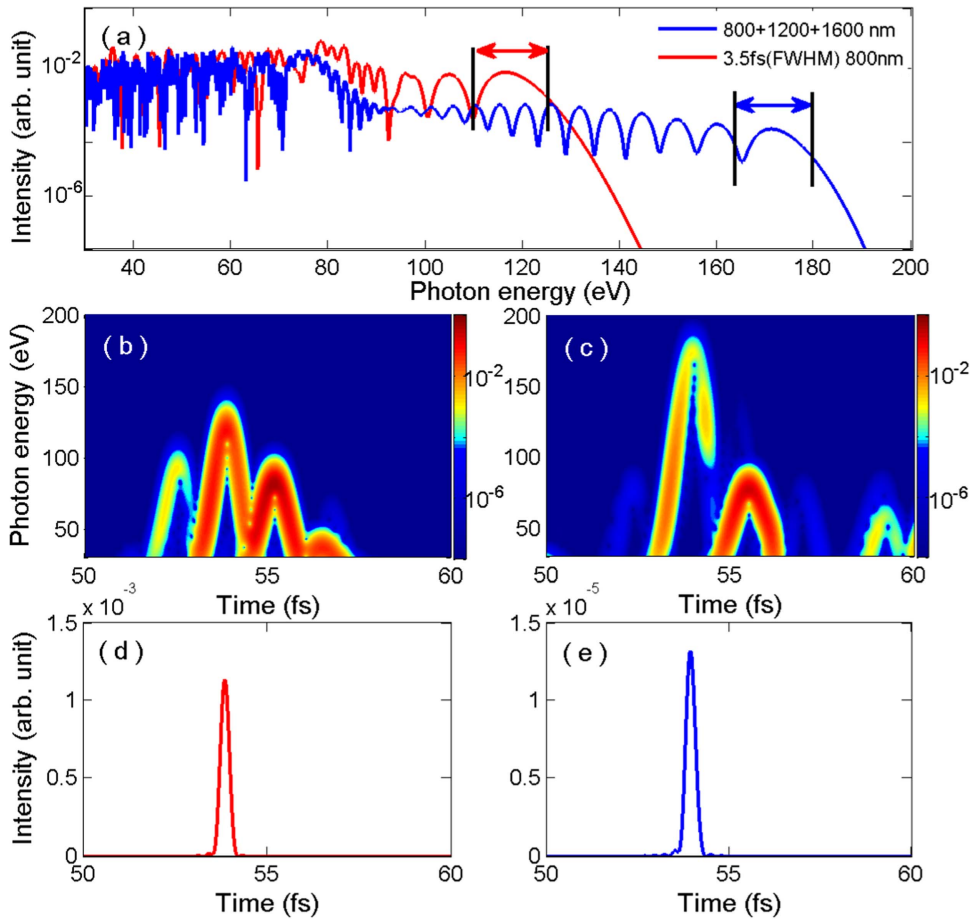

Figure 2. (a) Harmonic spectra driven by the laser fields shown in figure 1(a) (red curve) and figure 1(b) (blue curve). (b and c) The corresponding time-frequency analysis of the harmonic spectra shown in panel a by red and blue curves, respectively. (d and e) Attosecond pulses filtered from the harmonic spectra shown in panel a by red and blue curves, respectively. The selected harmonics are indicated by the double arrows in panel a.

the intensities and wavelengths of the second and third components of the three-color field, we find that the few-cycle-like structure can be obtained in a wide range of the intensities and wavelengths.

To demonstrate the few-cycle-like property of these synthesized fields, we take the three-color field of 800 nm + 1200 nm + 1600 nm shown in figure 1(b) as an example. Ar atom is chosen as the target. Hence, the intensity of 1.5×10^{14} W cm^{-2} for the fundamental field is chosen to avoid significant ionization of Ar atom. The spectra for the electric field shown in figures 1(a) and (b) are presented by the red and blue curves in figure 2(a), respectively. The corresponding time-frequency spectra are also presented in figures 2(b) and (c). Similar to the case of one-color few-cycle field, a super-continuum spectrum indicated by a double arrow is obtained near the cutoff for the synthesized field. A broad quasi-continuum structure is also observed in the harmonic spectrum, due to the interference between the contributions coming from long and short trajectories. From the time-frequency spectra shown in figures 2(b) and (c), one can see that the emission time of the harmonics with high photon energy is well confined into a half cycle of the driving field, as in the case of one-color few-cycle field. Hence, the harmonic spectrum generated by the synthesized field shows similar features to that of one color few-cycle field. Therefore, a few-cycle-like field is obtained by combining three multi-cycle pulses. The major difference between the harmonic spectra generated by one-color and three-color fields is a broader bandwidth of the quasi-continuum observed in the case of the synthesized field. This is because the larger amplitude difference between the second and first highest peak of the electric field observed in the case of three-color field [31, 34]. By directly filtering the harmonics in the super-continuum, an isolated attosecond pulse is obtained, as shown in figures 2(d) and (e) for the one-color field and the synthesized field, respectively.

When the driving pulse for producing isolated attosecond pulse is synthesized by three-color laser fields, both the CEP of each component and the time delays between different colors need to be well controlled. Although the optical path difference can be stabilized to below 1 fs [35], it is still very important to investigate the stability of attosecond pulse with the variation of time delays. A shift of the time delay when doing experiment can lead to different waveform of the driving field from pulse to pulse, accordingly may lead to an unstable

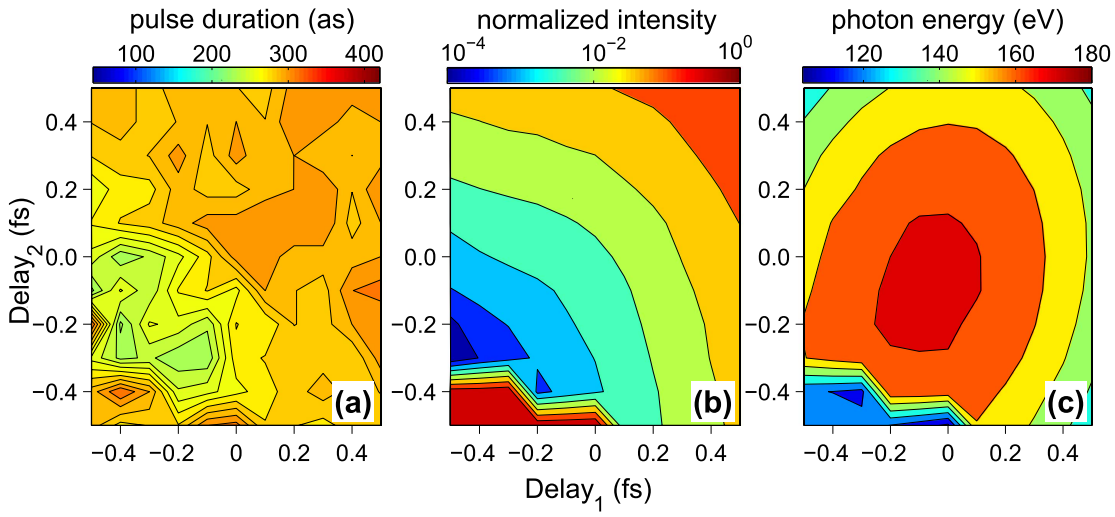

Figure 3. (a–c) The pulse durations (panel a), normalized intensities (panel b), and averaged photon energy (panel c) of the isolated attosecond pulses calculated by equation (5) (without phase compensation) as a function of delay$_1$ and delay$_2$ of the synthesized field. The other parameters of the driving field are the same as those used in figure 1(b). The dependence of the isolated attosecond pulse on delay$_1$ and delay$_2$ is characterized by the contour lines.

isolated attosecond pulse. In the following, we assume that the CEP of each component is stabilized and systematically investigate the sensitivity of the generated isolated attosecond pulse to the variation of time delay. We take the field shown in figure 1(b) as an example. delay$_1$ and delay$_2$ of the synthesized field vary from −0.5 fs to 0.5 fs. We first consider the case without phase compensation by using equation (5) to obtain the attosecond pulse. The higher photon energy ω_m of the selected harmonic spectrum is determined by one-order decay of the harmonic intensity compared with that of the plateau. The lower photon energy ω_n of the selected harmonic spectrum makes sure that the shortest isolated attosecond pulse is obtained for each time delay.

In figure 3, the pulse duration (panel a), the normalized intensity (panel b), and the averaged photon energy (panel c) of the obtained isolated attosecond pulse are presented as a function of delay$_1$ and delay$_2$. The pulse duration is defined by the full width at half maximum (FWHM). The intensities of the isolated attosecond pulses are normalized by the maximum value. The averaged photon energy of the attosecond pulse is calculated by using equation (7). The contour line is used to describe the sensitivity of the isolated attosecond pulse to the variation of time delay. As shown in figure 3(a), the pulse duration of the isolated attosecond pulse is in the range of 290 ± 10 as, when delay$_1$ and delay$_2$ vary from 0.0 fs to 0.5 fs. Whereas the variation of the pulse duration becomes significant, changing from 300 as to 230 as when delay$_1$ and delay$_2$ vary from −0.5 fs to 0.0 fs. Correspondingly, the contour line becomes very dense around −0.5 fs, as shown in figure 3(a). Hence, the attosecond pulse duration is very sensitive to the variation of delay$_1$ and delay$_2$ around −0.5 fs. Similar phenomenon is also observed for the normalized intensity and the photon energy of the isolated attosecond pulse, as presented in figures 3(b) and (c). When delay$_1$ and delay$_2$ vary from 0.5 fs to −0.5 fs, both the intensity and the photon energy change slowly at first, and then change significantly when delay$_1$ and delay$_2$ are close to −0.5 fs, as shown by the density of the contour line in figures 3(b) and (c). Hence, the isolated attosecond pulse, including its pulse duration, pulse intensity, and photon energy, is sensitive to the variation of delay$_1$ and delay$_2$ around −0.5 fs, while it is relatively stable from 0.0 fs to 0.5 fs.

To get an insight into the sensitivity of the isolated attosecond pulse to the variation of the time delay, we analyzed three typical cases of different time delays, i.e. delay$_1$ = delay$_2$ = −0.5 fs, delay$_1$ = delay$_2$ = 0.0 fs, and delay$_1$ = delay$_2$ = 0.5 fs. Their electric fields, the corresponding harmonic time-frequency spectra, and harmonic spectra are presented in the first, second, and third row of figure 4, respectively. The first, second, and third column correspond to the results for the case of delay$_1$ = delay$_2$ = −0.5 fs, delay$_1$ = delay$_2$ = 0.0 fs, and delay$_1$ = delay$_2$ = 0.5 fs, respectively. Because the isolated attosecond pulse is obtained by filtering the super-continuum spectrum in the cutoff, we just focus on the harmonic emission in the cutoff. There are two peaks of the electric field that play an important role in the harmonic emission in the cutoff. We denote these two peaks as 'A' and 'B' in figures 4(a1)–(a3). In the case of delay$_1$ = delay$_2$ = −0.5 fs shown in the first column of figure 4, the harmonics in the cutoff are mainly contributed by the electron ionized around peak 'B'. Hence, the harmonics are mainly emitted around 55.4 fs. As for the cases of delay$_1$ = delay$_2$ = 0.0 fs and delay$_1$ = delay$_2$ = 0.5 fs, the harmonics in the cutoff are emitted by the electron ionized around the peak 'A'. Hence, the emission time of the cutoff harmonics are around 54 fs, as shown in figures 4(b2) and (b3). When delay$_1$ and delay$_2$ vary from 0.5 fs to −0.5 fs, the harmonics in the cutoff is always contributed by the electron ionized

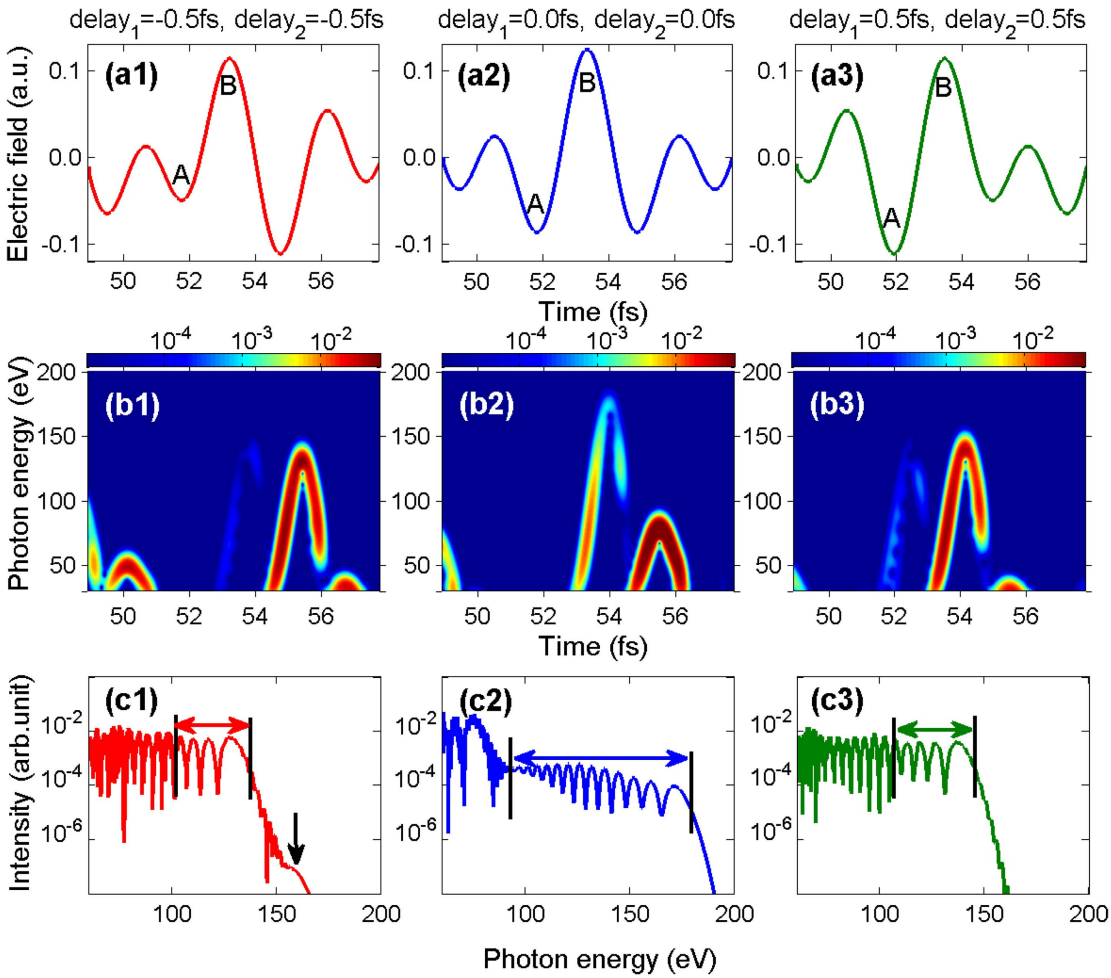

Figure 4. (a1–a3) The electric field of the synthesized pulse for three typical cases of different time delays. The first, second, and third column correspond to the case of $\text{delay}_1 = \text{delay}_2 = -0.5$ fs, $\text{delay}_1 = \text{delay}_2 = 0.0$ fs, and $\text{delay}_1 = \text{delay}_2 = 0.5$ fs, respectively. (b1–b3) The corresponding time-frequency spectra for the three typical cases of different time delay. (c1–c3) The corresponding harmonic spectra for the three typical cases of different time delay.

around peak 'A'. Until delay_1 and delay_2 are close to -0.5 fs, the harmonics in the cutoff turn to being contributed by the electron ionized around peak 'B'. Since the synthesized field possesses a few-cycle-like structure, the amplitudes of peak 'A' and 'B' are quite different. This leads to quite different properties of the harmonics emitted around 54 fs and 55.4 fs, including the harmonic phase, intensity, and photon energy. As a result, the isolated attosecond pulse obtained by filtering the cutoff present sharp changes in the pulse duration, intensity, and averaged photon energy around delays of -0.5 fs. From the above discussion, one can conclude that the shift of the harmonic emission time from a half cycle to another half cycle is the major cause of the sensitivity of the isolated attosecond pulse to the time delays around -0.5 fs.

By directly filtering a super-continuum cutoff from the harmonic spectrum, an isolated attosecond pulse can be obtained. This spectral range generally is narrow, as shown in figure 2(a). From the harmonic spectra shown in figures 4(c1)–(c3), one can see that besides the narrow super-continuum structure in the cutoff, a very broad quasi-continuum structure is also observed, as indicated by the double arrows. If there exists a certain relation between the harmonic phase and frequency for these broadband quasi-continuum spectra, then a broader spectral range can be selected to produce a shorter isolated attosecond pulse by applying phase compensation [23, 36]. Hence, in the following, we perform a detailed phase analysis of the harmonics to find the broadest spectral range where the phase compensation can be implemented. As examples, the harmonic phases of the spectra for the three typical cases discussed in figure 4 are presented in figures 5(a)–(c). The horizontal axis stands for the photon energy in eV unit. We use double lines to depict the spectral range of the quasi-continuum. As shown in figures 5(a)–(c), the harmonic phase presents a random behavior for the first tens of harmonic order, due to the interference between the harmonics emitted at different optical cycles. Whereas for the harmonics in the quasi-continuum, a piecewise-linear relation between the harmonic phase and the photon energy is observed in both cases of $\text{delay}_1 = \text{delay}_2 = -0.5$ fs and $\text{delay}_1 = \text{delay}_2 = 0.5$ fs. Several break points occurring in the middle of the piecewise-linear lines correspond to the spectral minima. In the case of

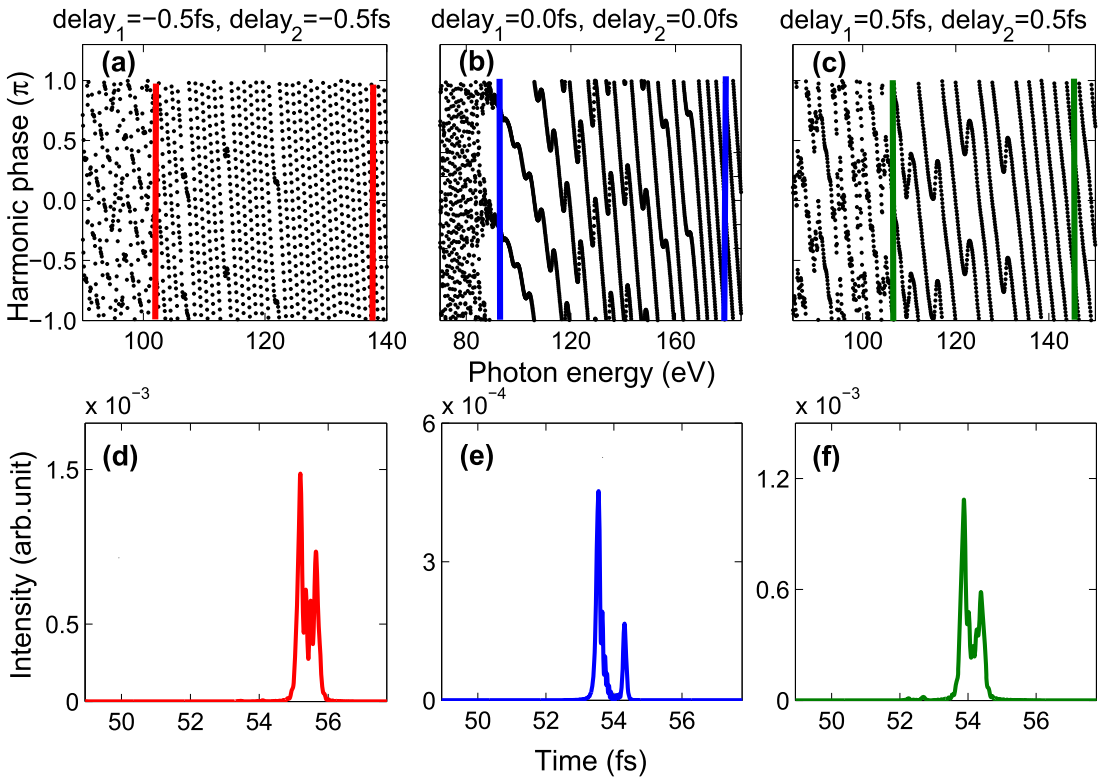

Figure 5. (a–c) The phase of the harmonic spectra shown in figures 4(c1)–(c3). (d–f) The attosecond pulses produced by filtering the quasi-continuum spectra indicated by the double lines in panels (a–c).

$\text{delay}_1 = \text{delay}_2 = 0.0$ fs, although a complicate behavior of the harmonic phase versus the photon energy is presented, the relation between them is also definite. We use equation (5) to calculate the attosecond pulse produced by filtering the quasi-continuum spectra. The results are shown in figures 5(d)–(f) for $\text{delay}_1 = \text{delay}_2 = -0.5$ fs, $\text{delay}_1 = \text{delay}_2 = 0.0$ fs, and $\text{delay}_1 = \text{delay}_2 = 0.5$ fs, respectively. As shown in figures 5(d)–(f), all the harmonics in the quasi-continuum are emitted within a half cycle of the fundamental field for all the three cases. In the case of $\text{delay}_1 = \text{delay}_2 = -0.5$ fs, the emission time is around 55.4 fs, while in the other two cases, the emission time is around 54.0 fs. This is consistent with the discussion on figure 4. The splits of these pulses are due to the different emission time of the harmonics contributed by the long and short trajectory. Hence, the phase of the harmonics emitted within only a half cycle presents a certain relation with the photon energy. This provides the possibility of phase compensation for these harmonics. Then a broader spectral range can be selected to produce a shorter isolated attosecond pulse.

In figure 6, the pulse duration (panel a), the pulse intensity (panel b), and the photon energy (panel c) of the isolated attosecond pulse with phase compensation are presented. The selected spectral range is determined by the phase analysis of the harmonics and is the broadest one where the relation between the harmonic phase and photon energy is definite. The intensity of the attosecond pulse shown in figure 6(b) is normalized by the maximum value. The contour line in figures 6(a)–(c) is used to characterize the dependence of the attosecond pulse on the time delays. For comparison, the scales of the color-maps are set to be the same as those in figure 3. As shown in figure 6(a), the attosecond pulse with phase compensation is significantly compressed into sub-hundred attosecond for most of the time delays. Since the selected harmonics include a part of the plateau, the averaged photon energy of the attosecond pulse with phase compensation is relatively lower than that of the attosecond pulse without phase compensation, as shown in figures 3(c) and 6(c). It is worth noting that, similar to the case without phase compensation, the attosecond pulse including its pulse duration, pulse intensity, and photon energy, is sensitive to the change of the time delay from $\text{delay}_1 = \text{delay}_2 = 0.0$ fs to $\text{delay}_1 = \text{delay}_2 = -0.5$ fs, while it is relatively stable from $\text{delay}_1 = \text{delay}_2 = 0.0$ fs to $\text{delay}_1 = \text{delay}_2 = 0.5$ fs, as shown by the contour lines in figure 6. Moreover, the stability of the attosecond pulse is better in the case with phase compensation.

To investigate the universality of the stabilization of the isolated attosecond pulse with few-cycle-like fields, we also considered the synthesized field with different wavelengths. In figure 7, the results for the case of 800 nm + 1300 nm + 1900 nm are presented. Other laser parameters are the same as those of the 800 nm + 1200 nm + 1600 nm field. The full characterization of the isolated attosecond pulse for the case

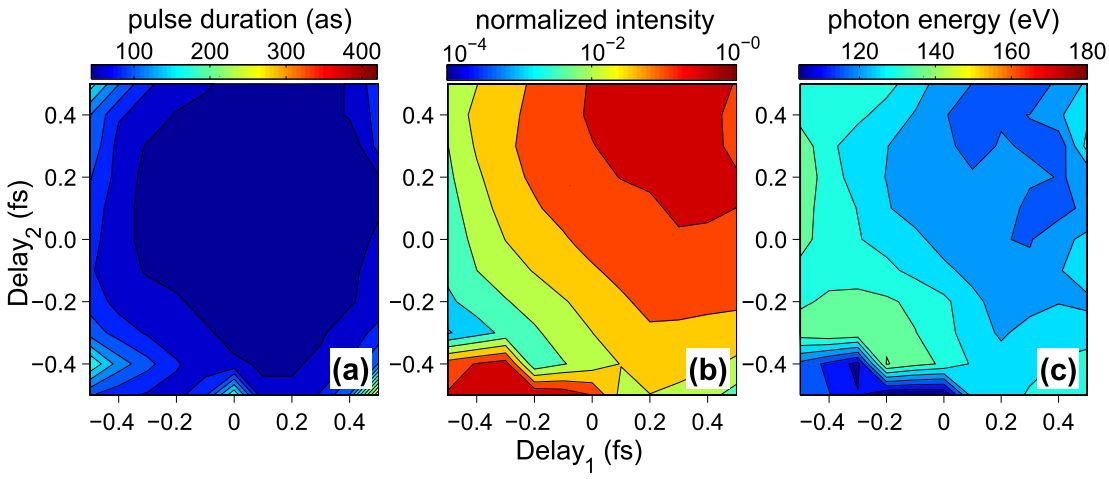

Figure 6. (a–c) The pulse durations (panel a), normalized intensities (panel b), and averaged photon energy (panel c) of the attosecond pulses calculated by equation (6) (with phase compensation) as a function of $delay_1$ and $delay_2$ of the synthesized field. The selected harmonic spectra are determined by the phase analysis of the harmonics and correspond to the broadest one where the phase compensation can be performed.

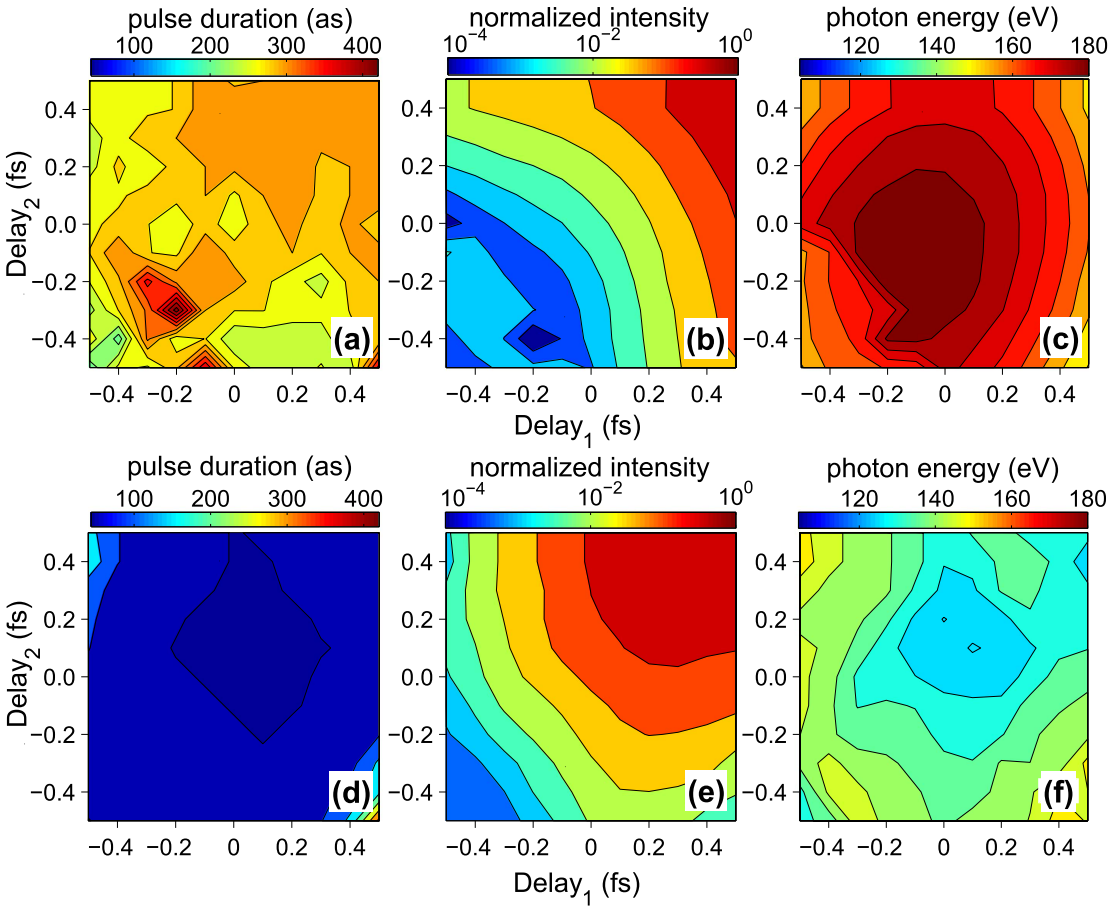

Figure 7. The pulse duration (the first column), the normalized intensity (the second column), and the averaged photon energy (the third column) of the isolated attosecond pulse for the case of mixing 800 nm, 1300 nm, and 1900 nm field. Other parameters of this synthesized field are the same as those of the case of mixing 800 nm, 1200 nm, and 1600 nm field. The first and second row correspond to the isolated attosecond pulse without and with phase compensation, respectively. The contour line is used to describe the stability of the properties of an attosecond pulse against the time delays.

without and with phase compensation are presented in the first and second row of figure 7, respectively. The first, second, and third column correspond to the pulse duration, the intensity, and the averaged photon energy of the isolated attosecond pulse, respectively. As shown in figure 7, the density of the contour line in panels (a–c),

panel (e), and panel (f) is lower in the top right corner than in the bottom left corner, while that in panel (d) is low for almost everywhere except for a small area in the bottom right corner. Hence, for both cases with and without phase compensation, the isolated attosecond pulses show a similar stability to those generated by the 800 nm + 1200 nm + 1600 nm field. In detail, for both cases with and without phase compensation, the attosecond pulse is relatively stable when $delay_1$ and $delay_2$ vary from 0.5 fs to 0.0 fs, while it becomes sensitive to the variation of $delay_1$ and $delay_2$ from 0.0 fs to −0.5 fs, especially around −0.5 fs.

4. Conclusion

In conclusion, we theoretically synthesized a few-cycle-like laser pulse by mixing three-color multi-cycle laser fields for the generation of isolated attosecond pulse. Then we investigate the dependence of the isolated attosecond pulse on the time delay between different-frequency components of the few-cycle-like three-color fields. Two cases without and with phase compensation are considered. To find the broadest spectral range where the phase compensation can be implemented, a detailed phase analysis is also performed. With the phase compensation, the durations of the isolated attosecond pulses can be significantly compressed into sub-hundred attosecond. Moreover, the isolated attosecond pulses without and with phase compensation are stable in the same window of time delay. By analyzing the variation of the electric field and the harmonic emission time with the time delays, the stability of the isolated attosecond pulse is well explained. To obtain a relatively stable attosecond pulse, one need to avoid the delays around which the emission time of the harmonics used to synthesize attosecond pulse shifts from a half cycle to another half cycle of the fundamental field. Hence, by confining the harmonic emission time in a half-cycle, the sensitivity of an isolated attosecond pulse to the shift of time delays can decrease, which is important to the ultrafast measurement with an isolated attosecond pulse.

Acknowledgments

This research has been supported in part by Global Research Laboratory Program [Grant No 2009-00439], by Max Planck POSTECH/KOREA Research Initiative Program [Grant No 2016K1A4A4A01922028] through the National Research Foundation of Korea (NRF), and by the National Natural Science Foundation of China [Grant No.11604248].

ORCID iDs

M Qin https://orcid.org/0000-0001-9496-1686

References

[1] Hentschel M *et al* 2001 *Nature* **414** 509–13
[2] Eckle P *et al* 2008 *Science* **322** 1525–9
[3] Schultze M *et al* 2010 *Science* **328** 1658–62
[4] Kienberger R *et al* 2004 *Nature* **427** 817–21
[5] Tong A, Zhou Y and Lu P 2017 *Opt. Quant. Electron* **49** 77
[6] Ma X, Li M, Zhou Y and Lu P 2017 *Opt. Quant. Electron.* **49** 170
[7] Warrick E R *et al* 2016 *J. Phys. Chem.* A **120** 3165
[8] Bækhøj J E and Madsen L B 2016 *Phys. Rev.* A **94** 043414
[9] Haessler S, Caillat J and Salières P 2011 *J. Phys.* B **44** 203001
[10] Qin M and Zhu X 2017 *Opt. Laser Technol.* **87** 79–86
[11] Ghimire S *et al* 2011 *Nature Phys.* **7** 138–41
[12] Schubert O *et al* 2014 *Nat. Photon.* **8** 119–23
[13] Vampa G *et al* 2015 *Nature* **522** 462
[14] Locher R, Castiglioni L, Lucchini M, Greif M, Gallmann L, Osterwalder J, Hengsberger M and Keller U 2015 *Optica* **2** 405–10
[15] Baltuska A *et al* 2003 *Nature* **421** 611–5
[16] Goulielmakis E *et al* 2008 *Science* **320** 1614–7
[17] Kling M F and Vrakking M J J 2008 *Annu. Rev. Phys. Chem.* **59** 463–92
[18] Nisoli M, Sansone G, Stagira S and Silvestri S D 2003 *Phys. Rev. Lett.* **91** 213905
[19] Corkum P B, Burnett N H and Ivanov M Y 1994 *Opt. Lett.* **19** 1870–2
[20] Kovacev M *et al* 2003 *Eur. Phys. J.* D **26** 79–82
[21] Sola I J *et al* 2006 *Nat. Phys.* **2** 319–22
[22] Sansone G *et al* 2006 *Science* **314** 443–6
[23] Zhang C, Yao J and Ni J 2012 *Opt. Express* **20** 24642–9
[24] Zhao K, Zhang Q, Chini M, Wu Y, Wang X and Chang Z 2012 *Opt. Lett.* **37** 3891–3
[25] Jin C, Wang G, Wei H, Le A T and Lin C D 2014 *Nat. Commun.* **5** 4003
[26] Li L, Wang Z, Li F and Long H 2017 *Opt. Quant. Electron.* **49** 73
[27] Haessler S, Balčiunas T, Fan G, Andriukaitis G, Pugžlys A and Baltuška A 2014 *Phys. Rev.* X **4** 021028

[28] Feng L and Chu T 2011 *Phys. Lett.* A **375** 3641–8
[29] He L, Li Y, Zhang Q and Lu P 2013 *Opt. Express* **21** 2683–92
[30] Feng L, Duan Y and Chu T 2013 *Ann. Phys. (Berlin)* **525** 915–20
[31] Lewenstein M, Balcou P, Ivanov M Y, L'Huillier A and Corkum P B 1994 *Phys. Rev.* A **49** 2117
[32] Ling W, Geng X, Guo S, Wei Z, Krausz F and Kim D 2014 *J. Opt.* **16** 102002
[33] Hong Z, Zhang Q, Rezvani S A, Lan P and Lu P 2018 *Opt. Laser Technol.* **98** 169–77
[34] Corkum P B 1993 *Phys. Rev. Lett.* **71** 1994–7
[35] Kim J, Chen J, Cox J and Kärtner F X 2007 *Opt. Lett.* **32** 3519–21
[36] Ko D H, Kim K T, Park J, Lee J and Nam C H 2010 *New J. Phys.* **12** 063008